

Estimation of Vehicle Parameters and Road Friction Using Steering Torque and Wheel Speeds

Yao Li, Jianwu Zhang, Xiqiang Guan
 School of Mechanical Engineering
 State Key Laboratory for Mechanical System and Vibration
 Shanghai Jiao Tong University
 800 Dong Chuan Road, Shanghai, 200240
 China
 liyao21@sjtu.edu.cn

Abstract: - It is often difficult to measure all necessary parameters directly in the current stability control systems. This paper presents a nonlinear observer to estimate vehicle's yaw rate, lateral acceleration, tire side slip angles and the road friction coefficient based on the measurement signals of the Electric Power Steering (EPS) system and the Anti-lock Braking System (ABS). The performances of the designed nonlinear observer have been investigated by means of computer simulations and experimental tests under various conditions.

Key-Words: - Nonlinear observer; Brush tire model; Tire aligning moment; Steering torque; Wheel speeds

1 Introduction

Current stability control systems on production vehicles are limited because some useful parameters can't be measured directly (such as the tire slip angles and the road friction coefficient) or the prices of the necessary sensors are too high (such as the gyro). A significant amount of costs can be saved if the parameters can be estimated by using available signals [1-4].

Ahn and Takagi proposed an estimation method of road friction, but it was difficult to detect the peak value of tire aligning moment [5, 6]. Ahn and Hsu suggested a nonlinear observer to estimate road friction and tire slip angles, but additional sensors were needed to measure the vehicle's yaw rate and lateral acceleration [7, 8]. C. Liu designed a modified adaptive observer and a least square algorithm to estimate the road surface condition, but the accuracy was not good enough in some cases [9]. Paul J. TH. et al used Kalman filters to detect the yaw rate, the lateral acceleration and the tire slip angles, however, the estimation model was based on a linear tire model which may reduce the accuracy of the results [10, 20].

In this paper, we first build a brush tire model according to a series of experimental results. Based on the measurement signals of the Electric Power Steering (EPS) system and the Anti-lock Braking System (ABS), a nonlinear observer is designed for estimation of several useful vehicle parameters and road friction coefficient. Finally, the performances

of the nonlinear observer have been investigated by means of computer simulations and experimental tests under various conditions.

2 Vehicle model

A simple two degrees of freedom vehicle model is established based on the nonlinear brush tire model and the EPS system model.

2.1 Tire model

The brush tire model (BTM) is a function of tire side slip angle α and tire-road friction coefficient μ [11]. The formula of this brush tire model reads:

$$F_y = \begin{cases} -3\mu F_z \gamma \{1 - |\gamma| + \frac{1}{3}(\gamma)^2\}, & |\alpha| \leq \alpha_{sl} \\ -\mu F_z \operatorname{sgn}(\alpha) & , \text{otherwise} \end{cases} \quad (1)$$

$$M_z = \begin{cases} \frac{l}{2} \mu F_z \gamma (1 - |\gamma|)^3, & |\alpha| \leq \alpha_{sl} \\ 0 & , \text{otherwise} \end{cases} \quad (2)$$

where $\gamma = \theta_y \tan(\alpha)$, $\theta_y = C_{\alpha f} / (3\mu F_z)$ and F_z is the tire normal force. $C_{\alpha f}$ is the tire cornering stiffness. l is the tire contact length and α_{sl} is the slip angle at which full tire slip occurs, $\alpha_{sl} = \tan^{-1}(1/\theta_y)$. F_y and M_z are the tire lateral force and aligning moment respectively.

In order to verify the brush tire model, especially the tire cornering characteristics, experiments were carried out on a single wheel test bed, shown in Fig. 1. Considering the precision of the Magic-Formula tire model (MFTM), the results of MFTM were also added for comparison [11]. The wheel speed was about 18 km/h and the tire pressure was 220KPa.



Fig. 1 Single wheel test bed

Figure 2 and Figure 3 show the lateral force and the aligning moment as a function of the tire side slip angle, respectively. Though the results of MFTM are a little better than those of BTM, BTM is excellent enough to describe the lateral characteristics of the tire. Comparing the lateral force with the aligning moment under the same vertical wheel load, it is easily find that the corresponding tire side slip angle of the maximum aligning moment is smaller than that of the maximum lateral force. In other words, the aligning moment is earlier than the lateral force to reach the peak value. That means it will be helpful if the information of the aligning moment is added into the estimation model.

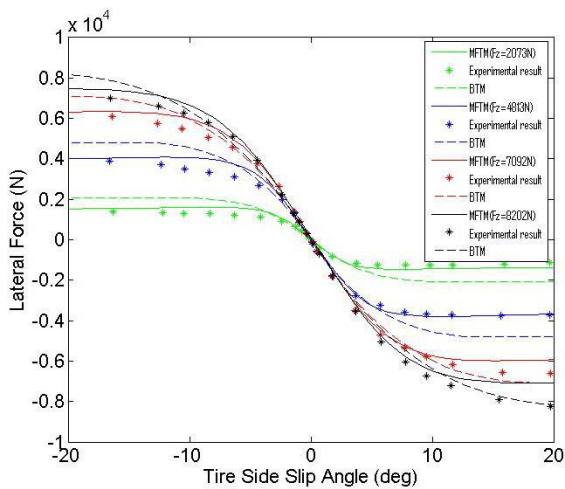


Fig. 2 Comparison of lateral force

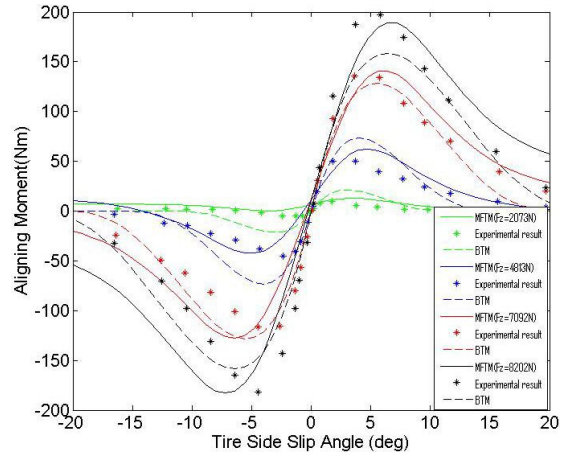


Fig. 3 Comparison of aligning moment

2.2 Steering system model

In the above section, we find that it will be helpful if we can obtain the information of the tire aligning moment. Unfortunately, the tire aligning moment M_z is hard to be measured directly. However, the total aligning moment of the steering system M_a can be calculated by the steering system model, especially with the help of the EPS system.

As the acting point of the lateral force on the front wheel is shifted slightly behind the contact surface centerline, it is common that the intersecting point of the line extending from the kingpin shaft and the ground is always at the front of the contact surface centerline, shown in Fig. 4. This figure shows that the moment arm of the lateral force is divided into two trails. The tire aligning moment is produced by the lateral force acting at the pneumatic trail ξ_p , while the total aligning moment is the result of the lateral force acting at both the pneumatic trail and the caster trail ($\xi_c + \xi_p$) [12].

Thus, M_a is

$$M_a = \sum_{i=l,r} -F_{yi} (\xi_{ci} + \xi_{pi}) = \sum_{i=l,r} -F_{yi} \xi_{ci} + M_{zi} \quad (3)$$

where i represents the left or right tire, ξ_c is the caster trail and ξ_p is the pneumatic trail.

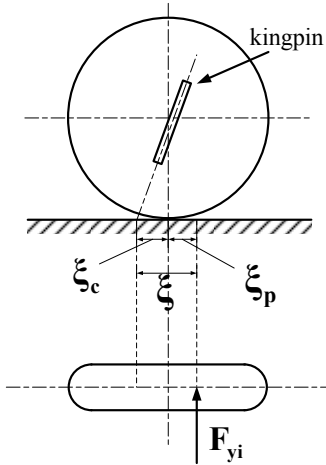


Fig. 4 Aligning moment on front wheel

Therefore, by utilizing the tire model introduced above to calculate the lateral force and the tire aligning moment, the total aligning moment can be estimated according to Eq. (3). Furthermore, the total aligning moment can also be measured indirectly based on the equilibrium of torque applied to steering system [13].

$$M_a = -[G_2(T_{sw} + G_1T_m + T_f) - J_r\ddot{\delta} - c_r\dot{\delta}] \quad (4)$$

where G_1 and G_2 are gear ratios of the reductor and the steering system, respectively, both of which are constants, T_{sw} is the steering torque applied by the driver which can be measured by the torque sensor equipped with EPS, T_m is the assist torque applied by the motor which is proportional to the motor current and T_f is the friction torque caused by the friction between various components of steering system which can be approximately calculated by the Coulomb friction law, J_r and c_r are the effective moment of inertia and the effective damping of the steering system, respectively, δ is the steering angle of the tire.

2.3 Vehicle model

Assuming a constant longitudinal speed, a simple two degrees of freedom vehicle model is established, shown in Fig. 5. This bicycle model effectively represents lateral and yaw dynamics of a two-axle ground vehicle with the following equations:

$$m(\dot{v} + u\omega_r) = (F_{yfl} + F_{yfr}) \cos \delta + F_{yrl} + F_{yrr} \quad (5)$$

$$I_z \dot{\omega}_r = a(F_{yfl} + F_{yfr}) \cos \delta - b(F_{yrl} + F_{yrr}) \quad (6)$$

where m is the entire vehicle mass, I_z is the moment inertia of the entire vehicle about vertical axis (z), a and b are the distances of the front and rear axles from CG, u and v are the longitudinal and lateral speed of the vehicle, respectively, ω_r is the yaw rate, F_{yfl} , F_{yfr} , F_{yrl} , F_{yrr} are the tire lateral forces of front left, front right, rear left and rear right tire, respectively.

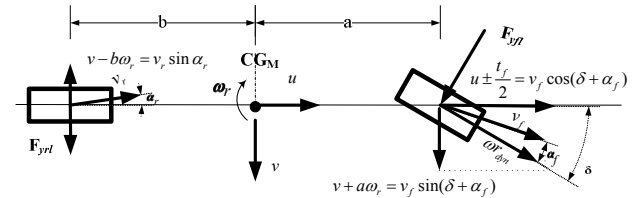


Fig. 5 Two degrees of freedom vehicle model

3 Nonlinear Observer

The nonlinear observer can be regarded as several virtual sensors because with the aid of a mathematical model and the particular measurement signals, unknown states can be estimated [10]. In this section, based on the measurement signals of EPS and ABS, a nonlinear observer is designed to estimate the vehicle's yaw rate, lateral acceleration, tire side slip angles and the road friction coefficient.

3.1 Observer design

Because of the symmetry of the bicycle model, the left and the right tires are assumed to have the same side slip angles which can be easily obtained by using simple kinematics:

$$\alpha_f = \frac{v + a\omega_r}{u} - \delta \quad (7)$$

$$\alpha_r = \frac{v - b\omega_r}{u} \quad (8)$$

where α_f and α_r are front and rear tire slip angles, respectively.

Differentiating Eq. (7) and Eq. (8) yields

$$\dot{\alpha}_f = \frac{\dot{v} + a\dot{\omega}_r}{u} - \dot{\delta} \quad (9)$$

$$\dot{\alpha}_r = \frac{\dot{v} - b\dot{\omega}_r}{u} \quad (10)$$

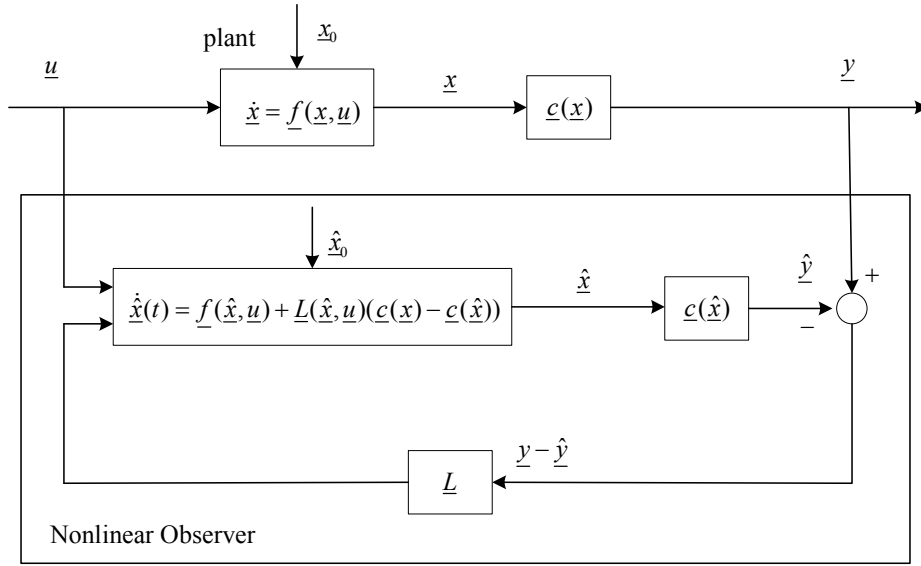


Fig. 6 Structure of the nonlinear observer from Zeitz

Based on the brush tire model and the bicycle model, the nonlinear state-space model can be given by:

$$\dot{v} = \frac{1}{m}(F_f + F_r) - u\omega_r \quad (11)$$

$$\dot{\omega}_r = \frac{1}{I_z}(aF_f - bF_r) \quad (12)$$

$$\dot{\alpha}_f = \left(\frac{1}{mu} + \frac{a^2}{I_z u}\right)F_f + \left(\frac{1}{mu} - \frac{ab}{I_z u}\right)F_r - \omega_r - \dot{\delta} \quad (13)$$

$$\dot{\alpha}_r = \left(\frac{1}{mu} - \frac{ab}{I_z u}\right)F_f + \left(\frac{1}{mu} + \frac{b^2}{I_z u}\right)F_r - \omega_r \quad (14)$$

$$\dot{\mu} = 0 \quad (15)$$

Because the above system is in nonlinear form, Zeitz's method is used here to design the nonlinear observer [14]. The structure of the nonlinear observer from Zeitz is shown in Fig. 6.

Eq. (11) ~ Eq. (15) can be brought into the standard form as:

$$\dot{\underline{x}} = \underline{f}(\underline{x}, \underline{u}) \quad (16)$$

$$\underline{y} = \underline{c}(\underline{x}) \quad (17)$$

The states and measurements are defined as follows:

$$\underline{x} = (v, \omega_r, \alpha_f, \alpha_r, \mu)^T \quad (18)$$

$$\underline{y} = (v + \left(\frac{a-b}{2}\right)\omega_r, \omega_r, M_a)^T \quad (19)$$

The state observation can then be given by:

$$\begin{aligned} \dot{\hat{\underline{x}}} &= \underline{f}(\hat{\underline{x}}, \underline{u}) + \underline{L}(\hat{\underline{x}}, \underline{u})(\underline{y} - \hat{\underline{y}}) \\ \hat{\underline{y}} &= \underline{c}(\hat{\underline{x}}) \end{aligned} \quad (20)$$

where $\underline{L}(\hat{\underline{x}}, \underline{u})$ is observer gain matrix.

The key problem for this observer design is gain selection. The observer gain matrix $\underline{L}(\hat{\underline{x}}, \underline{u})$ must be specified such that the estimation error $\tilde{\underline{x}}(t)$ tends to 0 for $t \rightarrow \infty$:

$$\lim_{t \rightarrow \infty} \tilde{\underline{x}}(t) = \lim_{t \rightarrow \infty} (\underline{x}(t) - \hat{\underline{x}}(t)) = 0 \quad (21)$$

The error differential equation can be formed as:

$$\begin{aligned} \dot{\tilde{\underline{x}}}(t) &= \dot{\underline{x}}(t) - \dot{\hat{\underline{x}}}(t) \\ &= \underline{f}(\underline{x}, \underline{u}) - \underline{f}(\hat{\underline{x}}, \underline{u}) \\ &\quad - \underline{L}(\hat{\underline{x}}, \underline{u})(\underline{c}(\underline{x}) - \underline{c}(\hat{\underline{x}})) \end{aligned} \quad (22)$$

The solution of Eq. (22) can be used to determine whether or not the condition of Eq. (21) is satisfied. $\underline{f}(\underline{x}, \underline{u})$ and $\underline{c}(\underline{x})$ are then expanded around $\hat{\underline{x}}$ using the Taylor series expansion.

$$\underline{f}(\underline{x}, \underline{u}) \approx \underline{f}(\hat{\underline{x}}, \underline{u}) + \frac{\partial \underline{f}}{\partial \underline{x}}(\hat{\underline{x}}, \underline{u})(\underline{x} - \hat{\underline{x}}) \quad (23)$$

$$\underline{c}(\underline{x}) \approx \underline{c}(\hat{\underline{x}}) + \frac{\partial \underline{c}}{\partial \underline{x}}(\hat{\underline{x}})(\underline{x} - \hat{\underline{x}}) \quad (24)$$

where the Jacobian matrix $\frac{\partial \underline{f}}{\partial \underline{x}}$ is

$$\frac{\partial f}{\partial \underline{x}} = \begin{pmatrix} \frac{\partial f_1}{\partial x_1} & \frac{\partial f_1}{\partial x_2} & \dots & \frac{\partial f_1}{\partial x_5} \\ \frac{\partial f_2}{\partial x_1} & \frac{\partial f_2}{\partial x_2} & \dots & \frac{\partial f_2}{\partial x_5} \\ \vdots & \vdots & \dots & \vdots \\ \frac{\partial f_5}{\partial x_1} & \dots & \dots & \frac{\partial f_5}{\partial x_5} \end{pmatrix}_{5 \times 5} \quad (25)$$

Substituting Eq. (23) and Eq. (24) into Eq. (22) yields:

$$\begin{aligned} \dot{\tilde{x}}(t) &= \left(\frac{\partial f}{\partial \underline{x}}(\hat{x}, u) - \underline{L}(\hat{x}, u) \frac{\partial c}{\partial \underline{x}}(\hat{x}) \right) \tilde{x} \\ &= \underline{F}(\hat{x}, u) \tilde{x} \end{aligned} \quad (26)$$

where $\underline{F}(\hat{x}, u)$ is the observer dynamic matrix.

In order to make sure that the solution $\tilde{x}(t)$ of the estimation error differential equation tends to 0 for $t \rightarrow \infty$ for any initial conditions, $\underline{F}(\hat{x}, u)$ must be constant and its eigenvalues lie to the left of the $j -$ axis.

$$\underline{F}(\hat{x}, u) = \frac{\partial f}{\partial \underline{x}}(\hat{x}, u) - \underline{L}(\hat{x}, u) \frac{\partial c}{\partial \underline{x}}(\hat{x}) = \underline{G} \quad (27)$$

where \underline{G} is a constant matrix and is chosen as a diagonal matrix here

$$\underline{G} = \begin{pmatrix} \lambda_1 & & & & \\ & \lambda_2 & & & \\ & & \lambda_3 & & \\ & & & \lambda_4 & \\ & & & & \lambda_5 \end{pmatrix} \quad (28)$$

where $\lambda_1, \lambda_2, \lambda_3, \lambda_4$ and λ_5 are the five eigenvalues.

According to Eq. (27), the observer gain matrix $\underline{L}(\hat{x}, u)$ can be calculated as:

$$\underline{L}(\hat{x}, u) = \left(\frac{\partial f}{\partial \underline{x}}(\hat{x}, u) - \underline{G} \right) \left(\frac{\partial c}{\partial \underline{x}}(\hat{x}) \right)^+ \quad (29)$$

Because the matrix $\frac{\partial c}{\partial \underline{x}}(\hat{x})$ is in general non-square, the Moore-Penrose pseudo-inversion $\left(\frac{\partial c}{\partial \underline{x}}(\hat{x}) \right)^+$ is used here [15].

$$\text{With } \underline{\hat{y}} = \underline{c}(\hat{x}) = \begin{pmatrix} \hat{v} + \left(\frac{a-b}{2} \right) \hat{\omega}_r \\ \hat{\omega}_r \\ \hat{M}_a \end{pmatrix}, \quad \frac{\partial c}{\partial \underline{x}}(\hat{x})$$

can be defined as:

$$\frac{\partial c}{\partial \underline{x}}(\hat{x}) = \begin{pmatrix} 1 & \frac{a-b}{2} & 0 & 0 & 0 \\ 0 & 1 & 0 & 0 & 0 \\ 0 & 0 & M_1 & M_2 & M_3 \end{pmatrix} \quad (30)$$

$$\text{where } M_1 = \frac{\partial M_a}{\partial \alpha_f}, M_2 = \frac{\partial M_a}{\partial \alpha_r}, M_3 = \frac{\partial M_a}{\partial \mu}$$

The Moore-Penrose pseudo-inversion of $\frac{\partial c}{\partial \underline{x}}(\hat{x})$

can be calculated as:

$$\left(\frac{\partial c}{\partial \underline{x}}(\hat{x}) \right)^+ = \begin{pmatrix} 1 & -\frac{a-b}{2} & & & \\ 0 & 1 & & & \\ 0 & 0 & \frac{M_1}{M_1^2 + M_2^2 + M_3^2} & & \\ 0 & 0 & \frac{M_2}{M_1^2 + M_2^2 + M_3^2} & & \\ 0 & 0 & \frac{M_3}{M_1^2 + M_2^2 + M_3^2} & & \end{pmatrix} \quad (31)$$

Substituting Eq. (25) and Eq. (28) into

$\frac{\partial f}{\partial \underline{x}}(\hat{x}, u) - \underline{G}$ yields:

$$\begin{aligned} \frac{\partial f}{\partial \underline{x}}(\hat{x}, u) - \underline{G} &= \\ &= \begin{pmatrix} -\lambda_1 & -u & f_{13} & f_{14} & f_{15} \\ 0 & -\lambda_2 & f_{23} & f_{24} & f_{25} \\ 0 & -1 & f_{33} - \lambda_3 & f_{34} & f_{35} \\ 0 & -1 & f_{43} & f_{44} - \lambda_4 & f_{45} \\ 0 & 0 & 0 & 0 & -\lambda_5 \end{pmatrix} \end{aligned} \quad (32)$$

$$\begin{aligned} \text{where } f_{13} &= F_1 / m, & f_{14} &= F_2 / m, \\ f_{15} &= F_3, & f_{23} &= \frac{a}{I_z} F_1, & f_{24} &= -\frac{b}{I_z} F_2, \end{aligned}$$

$$\begin{aligned}
f_{25} &= \frac{a \cos \delta}{I_z} \frac{\partial F_{yf}}{\partial \mu} - \frac{b}{I_z} \frac{\partial F_{yr}}{\partial \mu}, f_{33} = \left(\frac{1}{\mu u} + \frac{a^2}{I_z u} \right) F_1, \\
f_{34} &= \left(\frac{1}{\mu u} - \frac{ab}{I_z u} \right) F_2, \\
f_{35} &= \left(\frac{1}{\mu u} + \frac{a^2}{I_z u} \right) \frac{\partial F_{yf}}{\partial \mu} \cos \delta + \left(\frac{1}{\mu u} - \frac{ab}{I_z u} \right) \frac{\partial F_{yr}}{\partial \mu}, \\
f_{43} &= \left(\frac{1}{\mu u} - \frac{ab}{I_z u} \right) F_1, \quad f_{44} = \left(\frac{1}{\mu u} + \frac{b^2}{I_z u} \right) F_2, \\
f_{45} &= \left(\frac{1}{\mu u} - \frac{ab}{I_z u} \right) \frac{\partial F_{yf}}{\partial \mu} \cos \delta + \left(\frac{1}{\mu u} + \frac{b^2}{I_z u} \right) \frac{\partial F_{yr}}{\partial \mu}, \\
F_1 &= \frac{\partial F_y}{\partial \alpha_f}, F_2 = \frac{\partial F_y}{\partial \alpha_r}, F_3 = \frac{\partial F_y}{\partial \mu}.
\end{aligned}$$

Therefore, the observer gain matrix $\underline{L}(\hat{x}, \underline{u})$ can be calculated by Eq. (29).

As mentioned in the beginning of this section, the designed nonlinear observer only uses the measurement signals of EPS and ABS. The measurement equation of the nonlinear observer is given by

$$\underline{y} = \begin{pmatrix} \frac{v_{fl} + v_{fr}}{4} \sin(\delta + \hat{\alpha}_f) + \frac{v_{rl} + v_{rr}}{4} \sin(\hat{\alpha}_f) \\ \frac{v_{fl} - v_{fr}}{2t_f} \cos(\delta + \hat{\alpha}_f) + \frac{(\omega_{rl} - \omega_{rr})r_d}{2t_r} \\ -[G_2(T_{sw} + G_1 T_m + T_f) - c_r \dot{\delta}] \end{pmatrix} \quad (33)$$

where

$$v_{ij} = \frac{\omega_{ij} r_d}{\cos(\hat{\alpha}_i)} \quad (i = f, r; j = l, r) \quad (34)$$

In Eq. (33), the estimated tire slip angles are used to correct the measurement vector. The wheel speed signals are obtained from ABS, while the hand wheel torque, the assist torque and the steering angular speed are measured by the existing sensors of EPS. It should be noted that the steering angular speed is proportional to motor rotational speed and therefore proportional to the motor back emf [6]. Furthermore, compared with Eq. (4), the second order time derivative of the steering angle is ignored in the measurement of total aligning moment.

3.2 Improvement of algorithm

Though the road friction coefficient μ can be obtained directly from the nonlinear observer, its accuracy is unsatisfactory, especially on the high friction road.

As mentioned in the first section, Ahn and Takagi have proposed a method for the estimation of tire-road friction coefficient based on maximum aligning moment [5, 6]. However, when tire side slip angles are unavailable, it is really difficult to detect the peak point of the aligning moment. Thus, Ahn just used this method to calculate the lower bound of μ . Although Takagi succeed in detecting the point approximately under some assumptions, the accuracy was still unsatisfactory.

Unlike their algorithms, the estimated tire side slip angles from the nonlinear observer can be used to detect the peak point of the aligning moment.

As discussed above, the total aligning moment M_a can be calculated by Eq. (3). Considering the front axle, Eq. (3) can be rewritten as

$$M_a = (-F_{yf} \xi_c + M_{zf}) \quad (35)$$

Substituting Eq. (1) and Eq. (2) into Eq. (35) yields

$$\begin{aligned}
M_a &= \mu F_{zf} \text{sign}(\gamma) [\{1 - (1 - |\gamma|)^3\} \xi_c \\ &\quad + \frac{l}{2} |\gamma| (1 - |\gamma|)^3] \quad (36)
\end{aligned}$$

In order to get the maximum total aligning moment $M_{a \max}$, the partial derivative of M_a with respect to $|\gamma|$ is calculated as:

$$\begin{aligned}
\frac{\partial M_a}{\partial |\gamma|} &= \mu F_{zf} \text{sign}(\gamma) (1 - |\gamma|)^2 \\ &\quad \cdot \left(\frac{l}{2} (1 - 4|\gamma|) + 3\xi_c \right) \quad (37)
\end{aligned}$$

Thus, M_a takes its peak value at

$$|\gamma| = \frac{1}{4} \left(1 + \frac{6\xi_c}{l} \right) \quad (38)$$

Substituting Eq. (38) into Eq. (36) yields

$$M_{a \max} = \mu F_{zf} \text{sign}(\gamma) \cdot f(\xi_c, l) \quad (39)$$

where,

$$\begin{aligned}
f(\xi_c, l) &= (1 + 6\xi_c) \cdot \\ &\quad \frac{(27l^3 + 134l^2 \xi_c - 156l \xi_c^2 + 72\xi_c^3)}{512l^3} \quad (40)
\end{aligned}$$

Thus,

$$\mu = \frac{M_{a \max}}{f(\xi_c, l) F_{zf} \text{sign}(\gamma)} \quad (41)$$

It should be noted that all the parameters in Eq. (41) can be obtained or calculated approximately without additional sensors. The tire contact length l can be calculated by considering the inherent characteristic of tire structure and the contact between elastomers [16]. The caster trail ξ_c is a function of steering geometry and can be determined by kinematics [8, 17]. The vertical load of front axle can be computed approximately according to the static load distribution and the maximum total aligning moment $M_{a\max}$ can be calculated by Eq. (4).

The above derivation process means the time when Eq. (38) is satisfied is the time when M_a reaches its peak value and μ can be calculated by Eq. (41) at that time.

However, there are also disadvantages of the maximum aligning moment method (MAMM). Because MAMM depends on the estimated tire side slip angles, the road friction $\hat{\mu}_{MAMM}$ estimated by MAMM can't be used as an input of the tire model because the additional dynamic interactions may lead to an error if the current estimates are far from the actual values. Besides, although we have introduced the way to find the point of the maximum M_a , the point may also be missed if the calculation step size is not small enough. Clearly, if we decrease the step size, the computation speed will be unsatisfied. Although there are new algorithms to reduce the computational cost [18, 19], in the present paper, $\hat{\mu}_{MAMM}$ is just used to revise $\hat{\mu}_{NO}$ which is estimated by the nonlinear observer. The revised road friction is then written as:

$$\hat{\mu} = k_1 \hat{\mu}_{NO} + k_2 \hat{\mu}_{MAMM} \quad (42)$$

where k_1 and k_2 are the weighting coefficients:

$$k_1 = (1 - \hat{\mu}_{MAMM}) \quad (43)$$

$$k_2 = \hat{\mu}_{MAMM} \quad (44)$$

Eq. (42) can compensate for the disadvantages of the nonlinear observer and improve the performance of the estimator. However, if $\hat{\mu}_{MAMM}$ is far from $\hat{\mu}_{NO}$, $\hat{\mu}_{MAMM}$ will be thought to be an erroneous result and only $\hat{\mu}_{NO}$ will be used as an output. It should be noted here that because the estimation of road friction only depends on the measured total aligning moment which may become false when the side slip angle exceeds a certain threshold, another modification is made to the estimation algorithm: when the estimator detect a full tire slip at any axle,

the friction estimation will be suspended and the last $\hat{\mu}$ will be held.

4 Simulation and experimental results

In order to verify the nonlinear observer, both simulations and experiments were performed under different kinds of conditions.

1. Simulation with changing μ

Because of the internal feedback loop of the nonlinear observer, the designed estimator is expected to perform well even when the road condition suddenly changes or full tire slip occurs.

The vehicle speed was about 45 km/h and the initial value of $\hat{\mu}$ was set to 0.6. The steer input was a sine wave with a magnitude of 120° . Table 2 shows the vehicle parameters used in the simulation.

Figure 7~11 give the estimation performances of the nonlinear observer. Figure 7 and 8 show clearly that the estimated lateral acceleration and yaw rate do match well with the references. The road friction coefficient changes from 0.8 to 0.5 at about $t=25s$ and full tire slip occurs on the low friction road. However, the estimated slip angles still match well with the references, shown in Fig. 9 and 10. Figure 11 displays the estimation results of the road friction by three different methods. It can be seen that all of the three results can converge to the reference immediately even if the road surface changes suddenly. However, the result of nonlinear observer fluctuates wildly on the high friction road and the maximum aligning moment method overestimates $\hat{\mu}$ on the low friction road. The revised $\hat{\mu}$ shows the best performance among the three methods.

Table 2 Vehicle Parameters

Parameter	Value	Unit
a	1.423	m
b	1.117	m
h	0.386	m
I_x	284.5	
I_z	2248.1	
m	1535	kg

2. Simulation of constant radius cornering

In order to test the stability of the estimator, a constant radius cornering simulation was performed. The vehicle speed was gradually increased from 20 km/h to 45 km/h at first and then decreased to 20 km/h again.

Figure 12~18 show the simulation results of the estimator while driving with a constant radius. The results illustrate that all the parameters can follow the changes of the corresponding references. Although a small underestimation is detected at a high level of lateral acceleration, the accuracy of the estimator is still satisfactory considering the potential low cost of this algorithm.

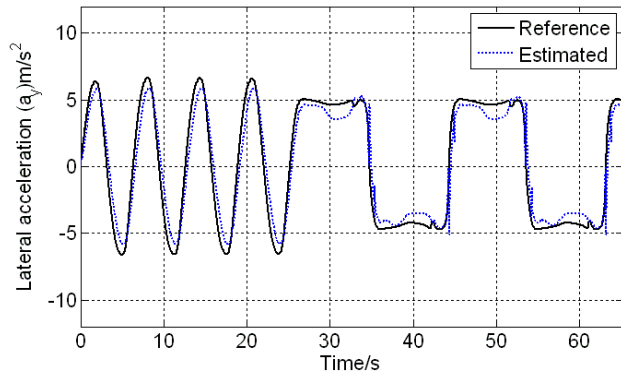


Fig. 7 Lateral acceleration on a changing friction road

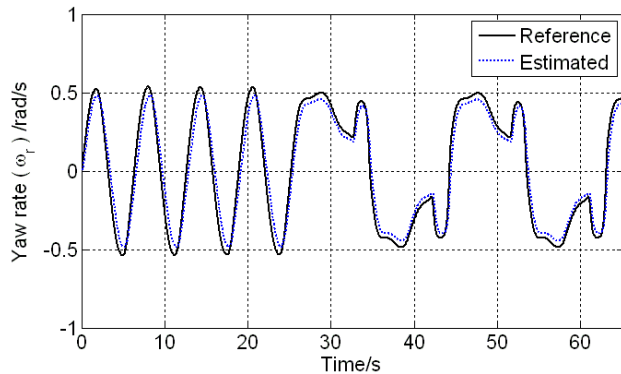


Fig. 8 Yaw rate on a changing friction road

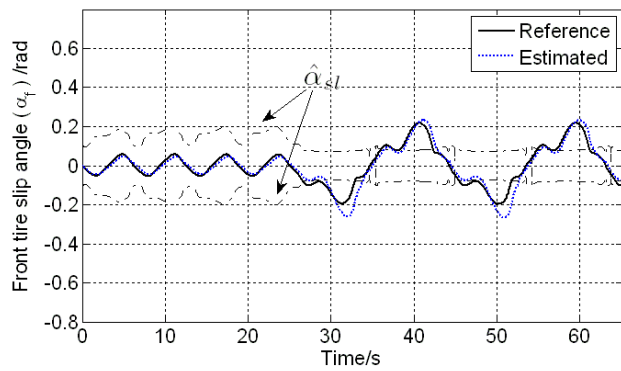


Fig. 9 Front tire slip angle on a changing friction road

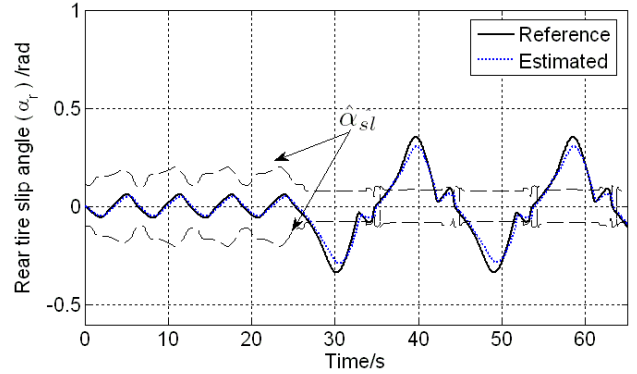


Fig. 10 Rear tire slip angle on a changing friction road

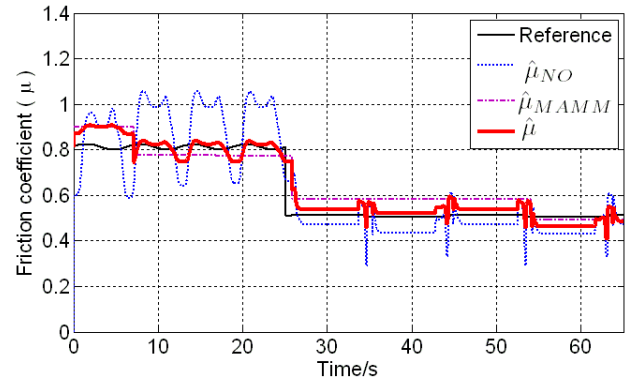


Fig. 11 Friction coefficient on a changing friction road

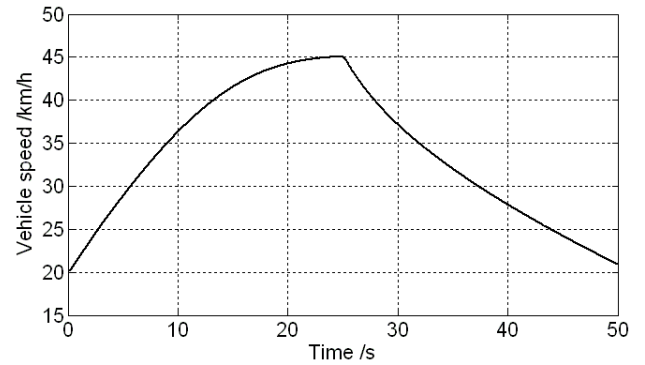


Fig. 12 Vehicle speed of constant radius cornering

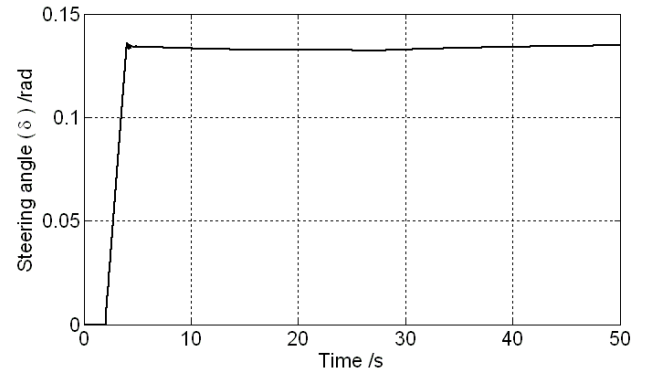


Fig. 13 Steering angle of constant radius cornering

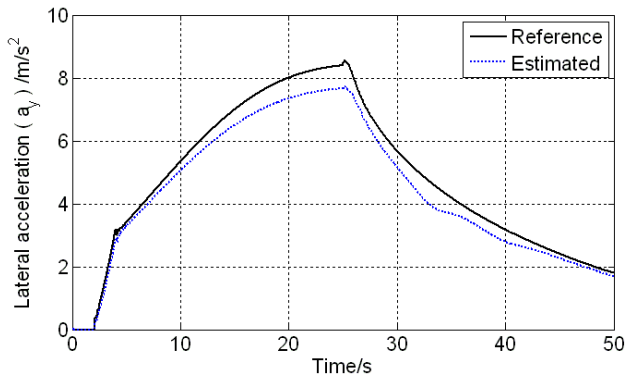


Fig. 14 Lateral acceleration of constant radius cornering

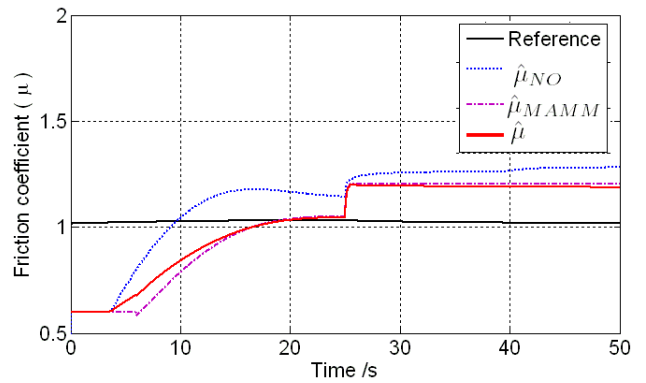


Fig. 18 Friction coefficient of constant radius cornering

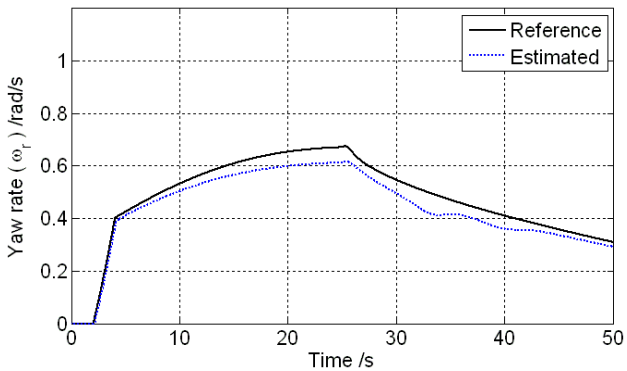


Fig. 15 Yaw rate of constant radius cornering

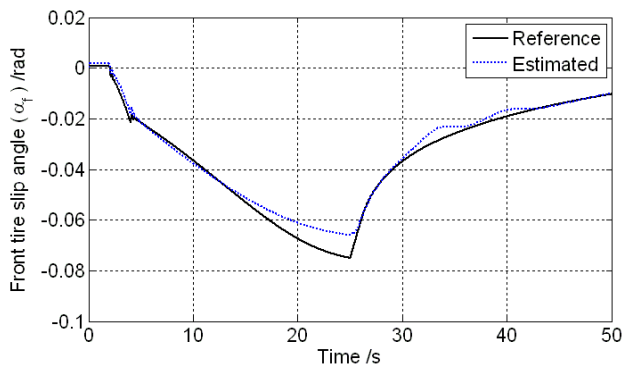


Fig. 16 Front tire slip angle of constant radius cornering

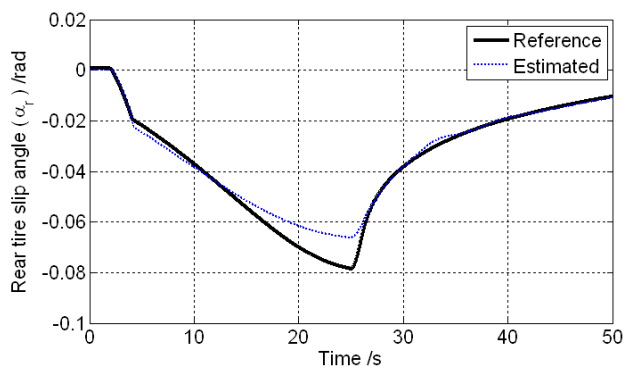


Fig. 17 Rear tire slip angle of constant radius cornering

3. Pylon Course Slalom Test

A pylon course slalom test was carried out on a high friction road. The friction coefficient of the test road was about 0.7~0.8 and the vehicle speed was around 60 km/h. The necessary data was measured and imported to the estimation model. Figure 19 ~22 show the nonlinear observer performances for the pylon course slalom test. The estimation results still demonstrate a good performance of this nonlinear observer.

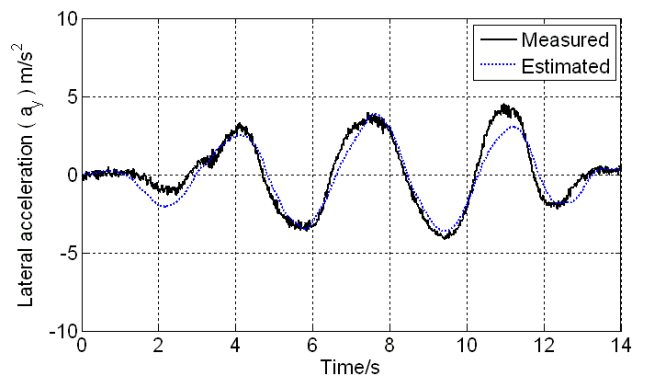


Fig. 19 Lateral acceleration of pylon course slalom test

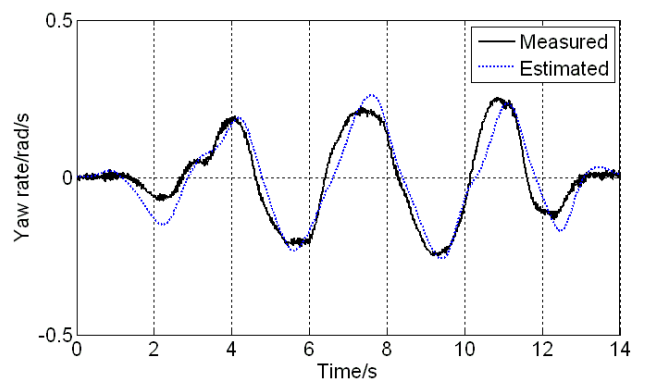


Fig. 20 Yaw rate of pylon course slalom test

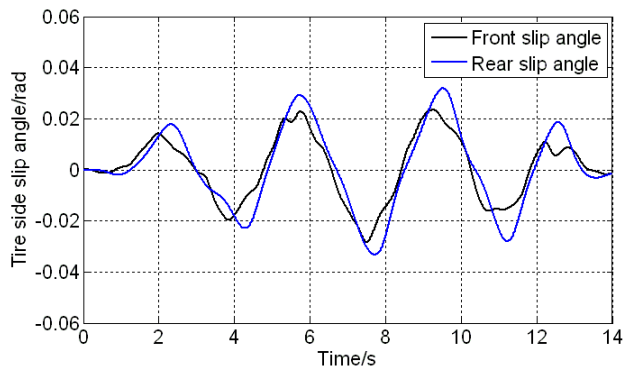


Fig. 21 Tire side slip angles of pylon course slalom test

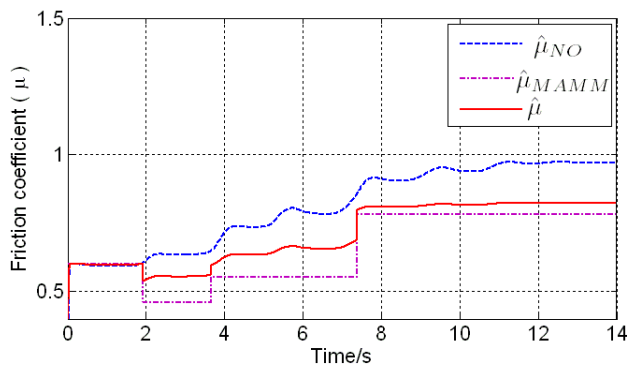


Fig. 22 Friction coefficient of pylon course slalom test

4 Conclusion

This paper presents a nonlinear observer for the estimation of vehicle parameters and road friction. The nonlinear observer has a cost advantage because it only utilizes the measurement signals of EPS and ABS which are available on many production vehicles. The designed nonlinear observer shows a good performance both in simulation and experiments.

Acknowledgement

The authors would like to acknowledge the financial supports to the research work by the National Natural Science Foundation of China under Grant No. 51175333

References:

- [1] Constantin Volosencu. Identification of Distributed Parameter Systems, Based on Sensor Networks and Artificial Intelligence, *WSEAS Traction on Systems*, issue 6, vol. 7, 2008, pp. 785-801.
- [2] Yan-e Zhao and Jianwu Zhang. Modeling and Simulation of the Electronic Differential System for an Electric Vehicle with Two-motor-wheel Drive, *International Journal of Vehicle Systems Modeling and Testing*, vol. 4, 2009, pp. 117-131.
- [3] Yan-e Zhao and Jianwu Zhang. Yaw Stability Control of a Four-independent-wheel Drive Electric Vehicle. *International Journal of Electric and Hybrid Vehicles*, vol. 2, No. 1, 2009, pp. 64-76.
- [4] Yan-e Zhao and Jianwu Zhang. Stability Control for a Four-independent-wheel Drive Electric Vehicle Based on Sliding Mode Control. *Shanghai Jiao Tong Daxue Xuebao*, vol. 43, No. 10, 2009, pp. 1526-1530.
- [5] C. Ahn et al. Estimation of Road Friction for Enhanced Active Safety Systems: Algebraic Approach. *2009 American Control Conference*, St. Louis, MO, USA, 2009.
- [6] F. Takagi et al. An Estimation Method of the Maximum Tire-road Friction Coefficient Using an Electric Power Assist Steering. *AVEC 2010*, 2010.
- [7] C. Ahn et al. Estimation of Road Friction for Enhanced Active Safety Systems: *Dynamic Approach*. *2009 American Control Conference*, St. Louis, MO, USA, 2009.
- [8] Y. Hsu et al. A Method to Estimate the Friction Coefficient and Tire Slip Angle Using Steering Torque. *2006 ASME International Mechanical Engineering Congress and Exposition*, Chicago, Illinois, 2006, pp. 1-10.
- [9] C. Liu and H. Peng. Road Friction Coefficient Estimation for Vehicle Path Prediction. *Vehicle System Dynamics*, 1996, pp. 413-425.
- [10] Paul J. Th. et al. Vehicle Dynamics Estimation Using Kalman Filters. *Vehicle System Dynamics*, 32, 1996, pp. 171-184.
- [11] H. B. Pacejka. Tire and Vehicle Dynamics. *Society of Automotive Engineers, Inc.*, 400 Commonwealth Dr. Warrendale, PA 15096-0001.
- [12] M. Abe. *Vehicle Handling Dynamics*. UK: Elsevier Ltd, 2009.
- [13] Deling Chen, Chengliang Yin and Jianwu Zhang. Controller design of a new active front steering system, *WSEAS Traction on Systems*, issue 11, vol. 7, 2008, pp. 1258-1268.
- [14] U. Kienche and L. Nielsen. *Automotive Control Systems*. Springer, 2005.
- [15] Yucai Su et al. *Matrix Theory*. Science Press, Beijing, 2006.

- [16] X. Zhu et al. Determination for Ground Contact Length and Static Radial Stiffness of Tire. *Tire Industry*, 1998, pp.458-461.
- [17] S. Laws et al. Steer-by-wire Suspension and Steering Design for Controllability and Observability. *IFAC World congress*, Prague, 2005.
- [18] Filippo Neri. Cooperative evolutive concept learning: an empirical study. *WSEAS Transaction on Information Science and Applications*, WSEAS Press (Wisconsin, USA), issue 5, vol. 2, 2005, pp. 559-563.
- [19] José De Jesus Rubio Avila, Andrés Ferreyra Ramírez and Carlos Avilés-Cruz. Nonlinear System Identification with a Feedforward Neural Network and an Optimal Bounded Ellipsoid Algorithm, *WSEAS Transaction on computers*, issue 5, vol. 7, 2008, pp. 542-551.
- [20] S. Malekzadeh et al. Optimal control of an 8-DOF vehicle active suspension system using Kalman observer. *International Journal of Shock and Vibration*, Volume 15, Number 5 / 2008, pp. 493-503.